

# Characterization of Genitourinary Lesions Using Diffusion-Weighted Imaging at 3T MRI

Farhood Saremi, M.D.<sup>1</sup>; Helmuth Schultze-Haakh, Ph.D.<sup>2</sup>

<sup>1</sup>Professor of Radiology and Medicine, University of California, Irvine (UCI), USA

<sup>2</sup>Siemens Medical Solutions USA, Cypress, CA, USA

There is growing interest in the application of diffusion-weighted imaging (DWI) for the evaluation of lesions in the abdomen and pelvis [1–3]. DWI yields both qualitative and quantitative information that can be helpful in differentiating benign from malignant processes. The application of DWI is useful for tumor detection, tumor characterization, and in the evaluation of tumor recurrence or response to treatment [4–7]. DWI has been widely used in neuroimaging [8–11]. However, its application to body imaging was initially limited by the inherent motion sensitivity of the technique coupled with the presence of bulk physiologic motion in the abdomen. Routine extracranial application of DWI has become feasible following a series of technological advancements in MR imaging. These developments include faster imaging techniques with echo-planar imaging (EPI) and parallel imaging,

high performance gradients, phased array multi-channel surface coils, and clinical use of higher magnetic field strengths [12–17]. Using new techniques, breathhold DWI sequences can be appended to existing imaging protocols without a significant increase in the total examination time. In this review, we describe our experience in using DWI for the characterization of genitourinary tract lesions as done on our MAGNETOM Trio, A Tim System with the Body Matrix coils.

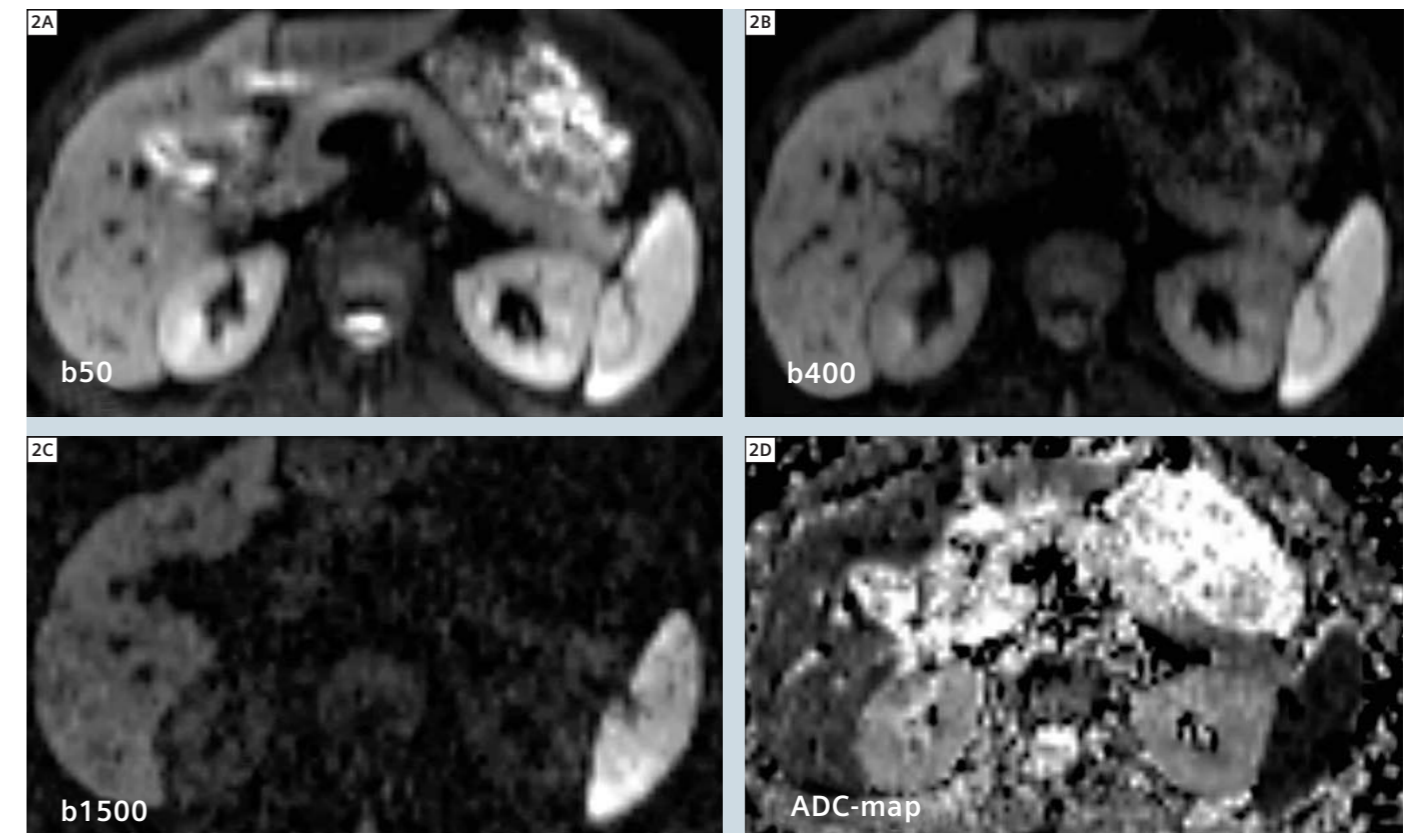
## Basic understanding of DWI technique

DWI sequences are designed to detect alterations in thermally-induced random (Brownian) motion of water molecules within tissues also known as diffusion [8, 9]. Diffusion effects are very small to be visible by conventional MRI. A DWI sequence requires the addition of a sym-

metric pair of diffusion-sensitizing gradients with opposed polarity [8, 9]. In contrast to static molecules, the random displacement of moving water molecules in the period between application of the first and second opposed polarity gradient pulses results in dephasing and consequent loss of signal intensity. The degree of signal loss is proportional to the degree of water motion (mean diffusional path length), with the highest signal attenuation seen with bulk water. The MR signal in DWI depends on two factors: the amplitude of random displacements of water molecules (related to the diffusion coefficient) and the b-value (the degree of diffusion-weighting). The optimal b-values for abdominal DWI have not yet been determined. DWI is typically performed using at least two b-values (within a range of 0 to 1000 s/mm<sup>2</sup>) to allow the calculation of the apparent diffusion coefficient (ADC).



**1** Breathhold diffusion-weighted images at b = 400 are obtained on our MAGNETOM Trio, A Tim System (with software version syngo MR B15) using fat suppressed single shot echo planar sequence without (A) and with (B) parallel imaging. scan time is 22 sec on both, and the field of view is 360 mm. TR is reduced from 3000 ms in A to 2600 ms in B and C. Two different parallel imaging techniques are used, syngo GRAPPA (A and B) and mSENSE (C). Spectral fat suppression is employed in all. Note the ghost artifact (long arrows) superimposed on the kidneys on the image without parallel imaging, which is pushed to the periphery following application of syngo GRAPPA and mSENSE. The overall image quality is clearly improved with parallel imaging. syngo GRAPPA is a preferred technique as aliasing artifacts are less frequent than with mSENSE (small arrows). Note: improved signal intensity in the center of the abdomen with syngo GRAPPA.



**2** Abdominal DWI – Normal Appearance. ADC of the kidney is the highest among all abdominal organs, followed by the liver, pancreas, and spleen. As the b-value increases, the signal of normal kidney drops. The spleen remains bright and liver signal decreases mildly. Note that the signal of the left liver lobe is generally lower than the right lobe (which may be caused by transmitted cardiac pulsations). The center of the abdomen generally has no signal mostly due to susceptibility effect of gastrointestinal air. The bright signal in the ADC-map is stomach content, not a solid organ.

As the b-value is increased, sensitivity to the effects of diffusion increases at the expense of longer TE and worsened signal-to-noise ratio (SNR) and image distortion.

## Imaging protocol at our institution

Most of the images shown herein were obtained using a 3 tesla (T) magnet (MAGNEOM Trio, Siemens Healthcare, Erlangen, Germany). We used a breathhold single-shot spin echo EPI combined with parallel imaging and spectral fat suppression [11–14]. Our DWI protocol is shown in Table 1.

In breathhold techniques, although the signal-to-noise ratio (SNR) is inferior compared with multiple averaging methods, the use of higher magnetic field strengths (e.g., 3 Tesla) and surface coils

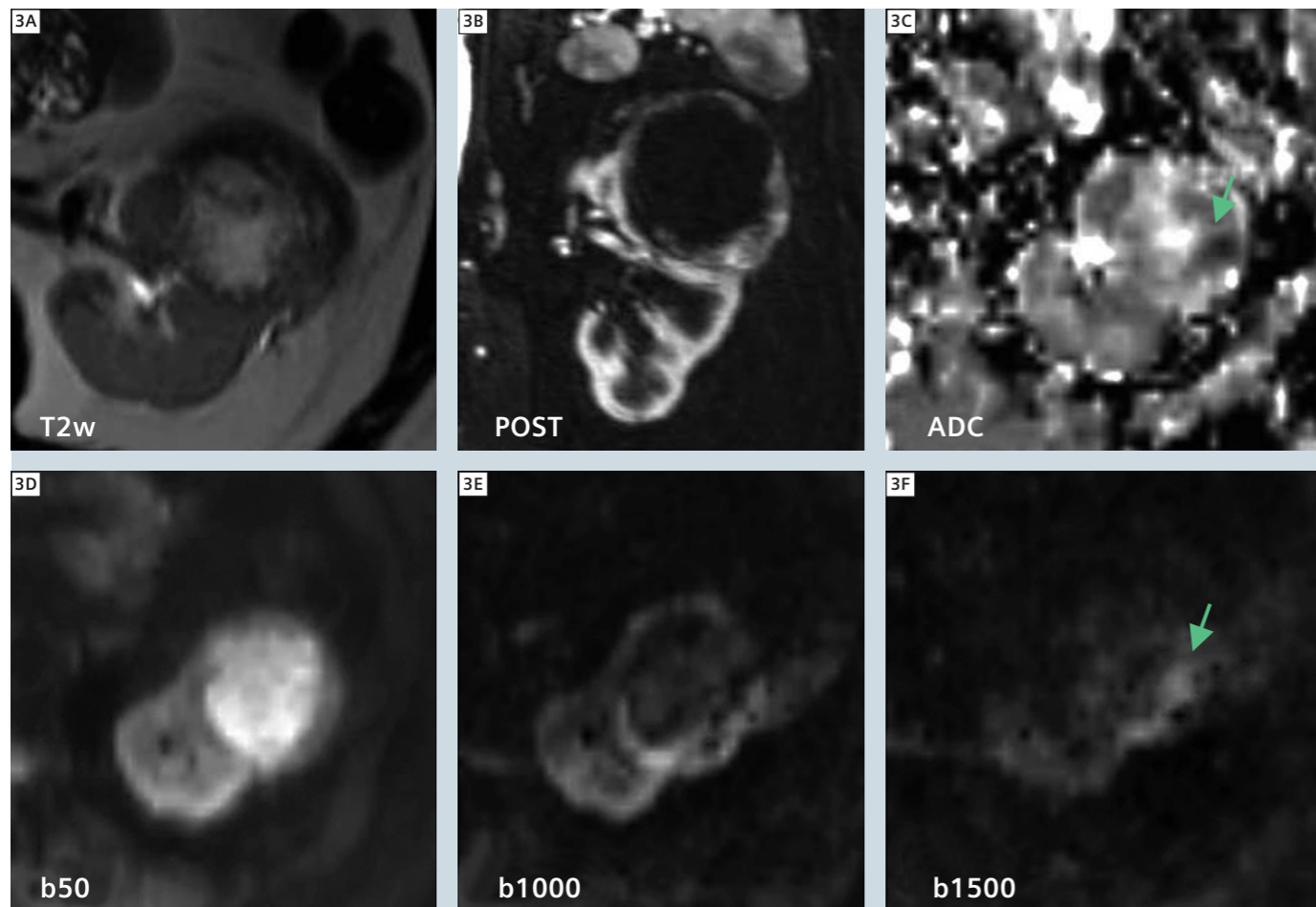
with more receiver channels (> 8) can compensate for poor SNR [17, 18]. We found spectral fat saturation technique more practical than STIR (short TI inversion recovery) for breathhold studies, since with STIR the acquisition time is longer and lesion visibility may be inferior compared with spectral fat saturation, especially in the center of the abdomen [19]. Parallel imaging is also essential for breathhold DW imaging. With parallel imaging, a shorter TE is possible which in fact increases the SNR and reduces susceptibility-induced image distortions [20–22] (Fig. 1). In our experience, syngo GRAPPA is more advantageous to mSENSE given the degree of off resonance and motion ghost artifacts associated with mSENSE (Fig. 1).

It is reported that the DW image quality is superior at 3T compared to 1.5 T and that

small lesions are better visualized [17]. 3T is particularly useful at higher b-values. However, with 3T we should expect larger susceptibility-induced image distortions and signal loss, and more motion-related artifacts [18]. Traditionally, most DWI studies have reported b-values of below 1000 s/mm<sup>2</sup>. However, the use of even greater b-values may be beneficial. For example, high grade tumors may retain their bright signal with b-values above 1000 s/mm<sup>2</sup>, whereas low grade tumors will lose their signal [23]. High b-values have also been used effectively to assess early recurrences of a tumor [24].

## Signal of normal tissues in DWI

The ADC of the kidney is the highest among all solid abdominal organs, followed by the liver, pancreas, and spleen [16, 25, 26] (Fig. 2). The ADC value of



**3** Cystic renal cell carcinoma. Axial T2-weighted (T2w) image of the left kidney demonstrates a large septated cystic lesion arising from the anterolateral margin of the left kidney. The bright signal intensity in the center of the lesion represents fluid. The anterior margin of the lesion shows lower signal intensity representing thickened fibrous capsule. The posterolateral margin of the lesion is mass-like and appears isointense to the normal renal parenchyma. Post contrast (post) image, DW images with b-values of 50, 1000, and 1500  $s/mm^2$ , and ADC-map image are shown. Note the bright signal intensity of the fluid portions of the lesion on the  $b = 50 s/mm^2$  image (related to T2 effects), as well as the bright signal intensity of the viable tumor on the  $b = 1500 s/mm^2$  image which appears low in signal on the ADC-map image (secondary to restricted diffusion). Biopsy of the hypercellular region showed renal cell carcinoma (long white arrow). Also note that on the post-contrast image both the fibrous capsule and tumor demonstrate enhancement.

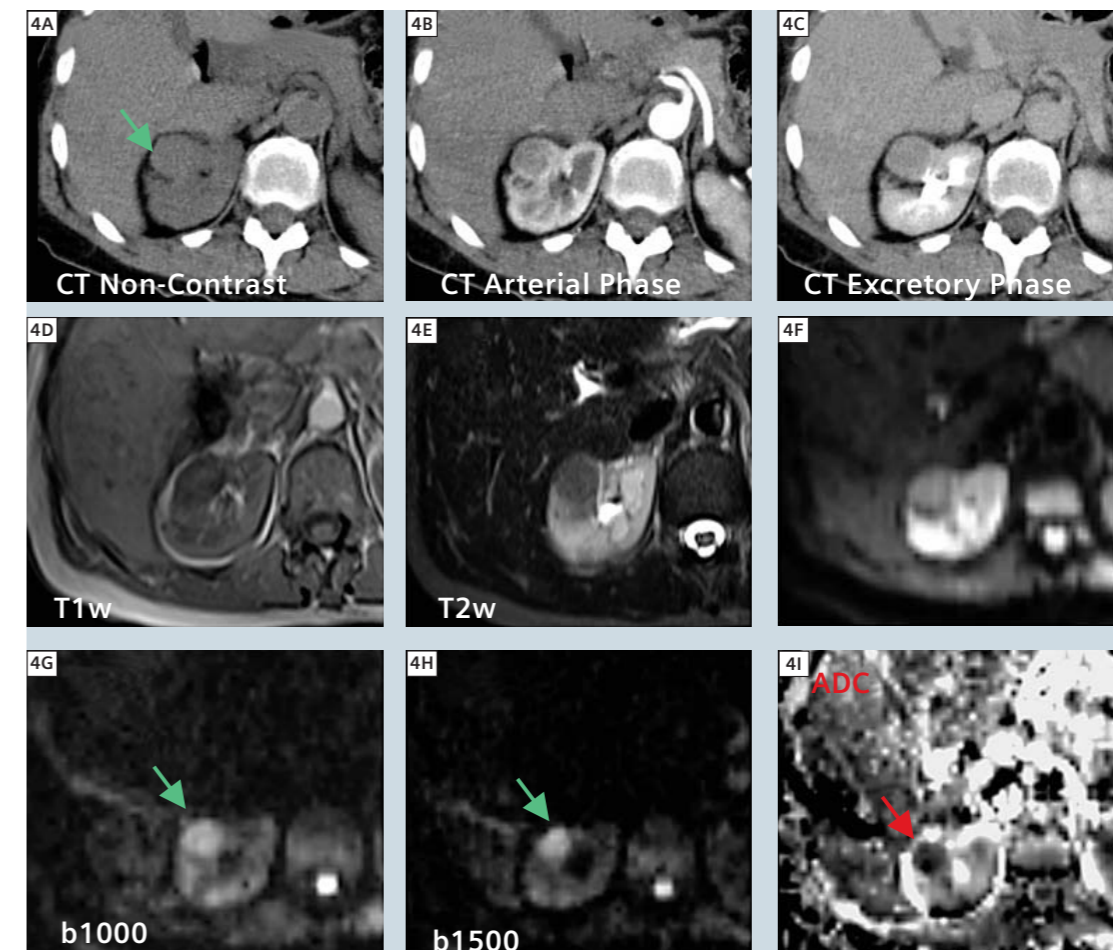
the renal cortex is generally higher than the medulla [27]. At high b-values, the signals from normal tissue such as blood vessels, muscle, and bowel will be suppressed. The kidneys, adrenal gland, and gallbladder lose their signal gradually and lose nearly all signal at  $b = 1000 s/mm^2$  and above. In contrast, some normal structures such as the spleen, prostate, testes, ovaries, endometrium, and spinal cord retain their bright signal at the higher b-values. Signal depletion in the center of the abdomen (pancreas) is common and likely related to susceptibility effects caused by gastrointestinal air. In the pelvis, the

endometrium and endocervix show the highest signal values and appear bright on all DWI series. Junctional zone (inner layer of myometrium) and cervical body demonstrate the lowest ADC values. In other words, both appear low in signal on  $b = 50 s/mm^2$  and bright on  $b = 1000$  to  $b = 1500 s/mm^2$ . Normal myometrium is intermediate signal on all b-values.

#### Assessment of cystic lesions

The signal intensity of most simple cysts drops significantly on  $b = 500 s/mm^2$  images and is lost completely on  $b = 1000-1500 s/mm^2$  images. The presence of blood products and high proteina-

cious material within a cyst may result in loss of signal on T2-weighted (T2w) and low b-value DWI images (compared with simple cysts) due to magnetic susceptibility effects of their contents. A similar effect can be seen with infected cysts and abscesses. ADC values of simple and complicated cysts are usually higher than solid lesions [28]. However, it should be noted that some overlap between the gross morphologic characteristics and ADC values of a complicated cyst and cystic renal cell carcinoma is not unusual. While needle biopsy is considered a relatively safe procedure, the incidence of



**4** 62-year-old male presented for evaluation of right renal mass. Computer Tomography (CT) images demonstrate mild enhancement of the mass on arterial phase and washout on the excretory phase. Further study with contrast enhanced MRI (three weeks later) showed mild enhancement on the arterial phase (image not shown) and heterogeneous signal on T1w and T2w images. DW images showed progressive signal enhancement of the mass (long arrows) with increasing b-values consistent with low ADC number. Percutaneous needle biopsy showed renal cell carcinoma. Radiofrequency ablation was performed.

complications is not negligible. In our experience with biopsy of cystic neoplasms, attention to findings provided by DWI can be very helpful in selecting biopsy sites to maximize the likelihood of positive results and may prevent an unnecessary repeat biopsy or surgery (Fig. 3).

#### Characterization of primary and metastatic tumors

DWI technique has been used successfully for the diagnosis and characterization of genitourinary lesions, including benign and malignant processes arising from the kidneys [29, 30], uterus [31], ovaries [32], and prostate [33], as well as for the detection of metastatic lesions in the liver, lymph nodes, and skeletal system [34–36]. Although ADC values have been demonstrated to differ significantly between benign and malignant lesions, it is not

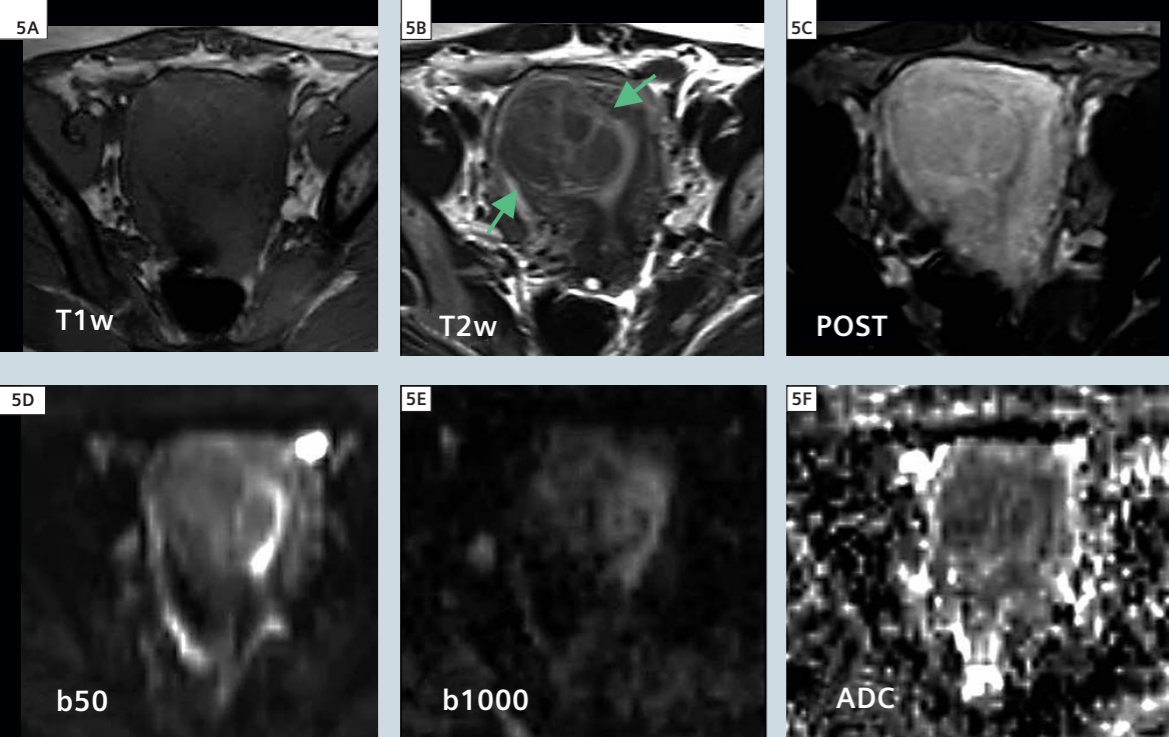
yet possible to confidently distinguish benign from malignant renal neoplasms on the basis of qualitative assessment of ADC measurements alone [37–40]. The degree of restriction to water diffusion in biologic tissue is inversely related to the tissue cellularity and the integrity of cell membranes [37–40]. As a consequence, diffusion is mostly restricted in highly cellular parts of a tumor because of a reduced extracellular space (Fig. 4). In contrast, diffusion is less restricted in hypocellular tumors and in tumors with glandular, necrotic, hemorrhagic, or cystic components (Fig. 3). In most benign processes such as cysts or benign masses of low cellularity (e.g., typical cavernous hemangioma), the signal intensity on DWI decays with increasing b-value. This results in high signal intensities of such benign lesions on the ADC-map [29]. In contrast, slower signal decay or even signal enhancement with

increasing b-values may indicate malignancy or viable hypercellular tissue (Fig. 4).

DWI and ADC-maps can be used to select optimal biopsy sites and to detect the presence of viable tumor on follow-up studies of patients after radiation or chemotherapy [41] (Fig. 3).

#### Pelvic masses

DWI performed with parallel imaging techniques has demonstrated potential as a method for differentiating benign from malignant pelvic lesions. Both endometrial cancer and normal endometrium appear hyperintense on DW images [42]. However, the ADC values of high grade endometrial cancers are lower than those of normal endometrium and low grade cancers. “Cellular” leiomyomas, composed of compact smooth muscle cells with little or no collagen, tend to be brighter on T2-weighted and DW images



**5** Benign cellular sub-endometrial fibroid in a 45-year-old patient (arrows). The mass demonstrates heterogeneous signal on DWI images with areas of mild restricted diffusion on ADC map consistent with hypercellularity. The tumor appears enhancing on post contrast (post) image. **Note:** high signal intensity of normal endometrium on all  $b = 50$  and  $b = 1000$   $s/mm^2$  values of DWI images.

(and darker on ADC images) compared with non-degenerated fibrous (collagenous) leiomyomas [31, 43, 44] (Fig. 5). The appearance of degenerated leiomyomas on DW images is quite variable. In patients with ovarian cancer, restricted diffusion is demonstrated not only at sites of primary malignancy but also in metastatic peritoneal implants [32].

It has been suggested in numerous reports that DWI together with T2w imaging can significantly improve identification of prostate cancers [33].

### Conclusions

DW imaging in combination with 3T equipment, is a robust method to facilitate the diagnosis of genitourinary

lesions with equivocal signal characteristics on routine MRI. It is not only helpful in differentiating benign from malignant processes, but can also be used as a tool for assessing possible tumor recurrence and to evaluate response to radiation treatment or chemotherapy on follow up scans.

### References

- Namimoto T, Yamashita Y, Sumi S, Tang Y, Takahashi M. Focal liver masses: characterization with diffusion-weighted echo planar MR imaging. *Radiology* 1997; 204: 739–44.
- Yamada I, Aung W, Himeno Y, Nakagawa T, Shibuya H. Diffusion coefficients in abdominal organs and hepatic lesions: evaluation with intravoxel incoherent motion echo-planar MR imaging. *Radiology* 1999; 210:617–623.
- Murtz P, Flacke S, Traber F, van den Brink JS, Gieseke J, Schild HH. Abdomen: diffusion-weighted MR imaging with pulse-triggered single-shot sequences. *Radiology* 2002;224 : 258–264.
- Herneth AM, Guccione S, Bednarski M. Apparent diffusion coefficient: a quantitative parameter for in vivo tumor characterization. *Eur J Radiol* 2003; 45: 208–13.
- Charles-Edwards EM, deSouza NM. Diffusion-weighted magnetic resonance imaging and its application to cancer. *Cancer Imaging*. 2006;6:135–43.
- Thoeny HC, De Keyzer F. Extracranial applications of diffusion-weighted magnetic resonance imaging. *Eur Radiol*. 2007;17(6):1385–93.
- Namimoto T, Awai K, Nakaura T, Yanaga Y, Hirai T, Yamashita Y. Role of diffusion-weighted imaging in the diagnosis of gynecological diseases. *Eur Radiol*. 2008 Oct 7. [Epub ahead of print].

- Le Bihan D, Breton E, Lallemand D, Grenier P, Cabanis E, Laval-Jeantet M. MR imaging of intravoxel incoherent motions: application to diffusion and perfusion in neurologic disorders. *Radiology* 1986; 161: 401–7.
- Le Bihan D, Breton E, Lallemand D, Aubin ML, Vignaud J, Laval-Jeantet M. Separation of diffusion and perfusion in intravoxel incoherent motion MR imaging. *Radiology* 1988; 168:497–505.
- Moseley ME, Kucharczyk J, Mintorovitch J, et al. Diffusion-weighted MR imaging of acute stroke: correlation with T2-weighted and magnetic susceptibility-enhanced MR imaging in cats. *AJNR Am J Neuroradiol* 1990; 11: 423–9.
- Rowley HA, Grant PE, Roberts TP. Diffusion MR imaging: theory and applications. *Neuroimaging Clin N Am* 1999; 9: 343–61.
- Müller MF, Prasad P, Siewert B, Nissenbaum MA, Raptopoulos V, Edelman RR. Abdominal diffusion mapping with use of a whole-body echo-planar system. *Radiology* 1994; 190:475–478.
- Chow LC, Bammer R, Moseley ME, Sommer FG. Single breath-hold diffusion-weighted imaging of the abdomen. *J Magn Reson Imaging* 2003; 18:377–382.
- Yamashita Y, Tang Y, Takahashi M. Ultrafast MR imaging of the abdomen: echo planar imaging and diffusion-weighted imaging. *J Magn Reson Imaging* 1998; 8:367–374.
- Okada Y, Ohtomo K, Kiryu S, Sasaki Y. Breathhold T2-weighted MRI of hepatic tumors: value of echo planar imaging with diffusion-sensitizing gradient. *J Comput Assist Tomogr* 1998; 22:364–371.
- Yoshikawa T, Kawamitsu H, Mitchell DG, et al. ADC measurement of abdominal organs and lesions using parallel imaging technique. *AJR Am J Roentgenol*. 2006;187(6):1521–30.
- Matsuoka A, Minato M, Harada M, et al. Comparison of 3.0- and 1.5-tesla diffusion-weighted imaging in the visibility of breast cancer. *Radiat Med*. 2008;26(1):15–20.
- Mürtz P, Krautmacher C, Träber F, Gieseke J, Schild HH, Willinek WA. Diffusion-weighted whole-body MR imaging with background body signal suppression: a feasibility study at 3.0 Tesla. *Eur Radiol*. 2007;17(12):3031–7.
- Wenkel E, Geppert C, Schulz-Wendtland R, et al. Diffusion weighted imaging in breast MRI: comparison of two different pulse sequences. *Acad Radiol*. 2007;14(9):1077–83.
- Taouli B, Martin AJ, Qayyum A, et al. Parallel imaging and diffusion tensor imaging for diffusion-weighted MRI of the liver: preliminary experience in healthy volunteers. *AJR Am J Roentgenol*. 2004;183(3):677–80.
- Naganawa S, Kawai H, Fukatsu H, et al. Diffusion-weighted imaging of the liver: technical challenges and prospects for the future. *Magn Reson Med Sci*. 2005;4(4):175–86.
- Skare S, Newbould RD, Clayton DB, Albers GW, Nagle S, Bammer R. Clinical multishot DW-EPI through parallel imaging with considerations of susceptibility, motion, and noise. *Magn Reson Med*. 2007;57(5):881–90.

- Alvarez-Linera J, Benito-León J, Escibano J, Rey G. Predicting the histopathological grade of cerebral gliomas using high b value MR DW imaging at 3-tesla. *J Neuroimaging*. 2008;18(3):276–81.
- Ichikawa T, Haradome H, Hachiya J, Nitatori T, Araki T. Diffusion-weighted MR imaging with single-shot echo-planar imaging in the upper abdomen: preliminary clinical experience in 61 patients. *Abdom Imaging*. 1999;24(5):456–61.
- Kilickesmez O, Yirik G, Bayramoglu S, Cimilli T, Aydin S. Non-breath-hold high b-value diffusion-weighted MRI with parallel imaging technique: apparent diffusion coefficient in normal abdominal organs. *Diagn Interv Radiol* 2008;14 (2): 83–87.
- Mardor Y, Pfeffer R, Spiegelmann R, et al. Early detection of response to radiation therapy in patients with brain malignancies using standard and high b-value diffusion-weighted MRI. *J Clin Oncol* 2003; 21:1094–1100.
- Zhang J, Tehrani YM, Wang L, Ishill NM, Schwartz LH, Hricak H. Renal masses: characterization with diffusion-weighted MR imaging—a preliminary experience. *Radiology* 2008;247(2):458–64.
- Cova M, Squillaci E, Stacul F, et al. Diffusion weighted MRI in the evaluation of renal lesions: preliminary results. *Br J Radiol* 2004; 77:851–857.
- Thoeny HC, De Keyzer F, Oyen RH, Peeters RR. Diffusion-weighted MR imaging of kidneys in healthy volunteers and patients with parenchymal diseases: initial experience. *Radiology* 2005; 235:911–917.
- Namimoto T, Yamashita Y, Mitsuzaki K, Nakayama Y, Tang Y, Takahashi M. Measurement of the apparent diffusion coefficient in diffuse renal disease by diffusion-weighted echo-planar MR imaging. *J Magn Reson Imaging* 1999; 9:832–837.
- Tamai K, Koyama T, Saga T, et al. The utility of diffusion-weighted MR imaging for differentiating uterine sarcomas from benign leiomyomas. *Eur Radiol*. 2008;18(4):723–30.
- Nakayama T, Yoshimitsu K, Irie H, et al. Diffusion-weighted echo-planar MR imaging and ADC mapping in the differential diagnosis of ovarian cystic masses: usefulness of detecting keratinoid substances in mature cystic teratomas. *J Magn Reson Imaging*. 2005;22(2):271–8.
- Morgan VA, Kyriazi S, Ashley SE, DeSouza NM. Evaluation of the potential of diffusion-weighted imaging in prostate cancer detection. *Acta Radiol*. 2007;48(6):695–703.
- Koh DM, Scurr E, Collins DJ, Pirgon A, Kanber B, Karanjia N et al. Colorectal hepatic metastases: quantitative measurements using single-shot echo-planar diffusion-weighted MR imaging. *Eur Radiol*. 2006;16(9):1898–905.
- Herneth AM, Philipp MO, Naude J, et al. Vertebral metastases: assessment with apparent diffusion coefficient. *Radiology* 2002; 225:889–894.
- Abdel Razek AA, Soliman NY, Elkhamary S, Alsharaway MK, Tawfik A. Role of diffusion-

- weighted MR imaging in cervical lymphadenopathy. *Eur Radiol*. 2006;16(7):1468–77.
- Sugahara T, Korogi Y, Kochi M, et al. Usefulness of diffusion-weighted MRI with echo-planar technique in the evaluation of cellularity in gliomas. *J Magn Reson Imaging* 1999; 9:53–60.
- Stadnik TW, Chaskis C, Michotte A, et al. Diffusion-weighted MR imaging of intracerebral masses: comparison with conventional MR imaging and histologic findings. *AJNR Am J Neuro-radiol*. 2001;22(5):969–76.
- Guo AC, Cummings TJ, Dash RC, Provenzale JM. Lymphomas and high-grade astrocytomas: comparison of water diffusibility and histologic characteristics. *Radiology*. 2002;224(1):177–83.
- Squillaci E, Manenti G, Cova M, et al. Correlation of diffusion-weighted MR imaging with cellularity of renal tumours. *Anticancer Res* 2004; 24:4175–4179.
- Razek AA, Megahed AS, Denewer A, Motamed A, Tawfik A, Nada N. Role of diffusion-weighted magnetic resonance imaging in differentiation between the viable and necrotic parts of head and neck tumors. *Acta Radiol*. 2008;49(3):364–70.
- Tamai K, Koyama T, Saga T, et al. Diffusion-weighted MR imaging of uterine endometrial cancer. *J Magn Reson Imaging*. 2007;26(3):682–7.
- Yamashita Y, Torashima M, Takahashi M, et al. Hyperintense uterine leiomyoma at T2-weighted MR imaging: differentiation with dynamic enhanced MR imaging and clinical implications. *Radiology* 1993; 189:721–725.
- Murase E, Siegelman ES, Outwater EK, Perez-Jaffe LA, Tureck RW. Uterine leiomyomas: histopathologic features, MR imaging findings, differential diagnosis, and treatment. *Radiographics*. 1999;19(5):1179–97.

**Table 1: Diffusion-Weighted Imaging protocol on MAGNETOM Trio with software version syngo MR B15.**

2D single shot spin echo EPI (EPI factor = 84)

**b-values:** 50, 400, 1000, and 1500  $s/mm^2$

**Body Matrix coils:** 8-channel, **BW:** 2056 Hertz/pixel

**Fat suppression:** normal Fat Sat

**TR/TE:** 2500–3000  $s/mm^2$  / 72 for b-values 50 and 1000, 2800–3000  $s/mm^2$  / 78 for b-values 400 and 1500  $s/mm^2$

**Total Imaging Time:** 21–24 sec for each set

**Matrix size:** 84 x 128

**Slice Thickness/Gap:** 5/1.5 mm, 20 slices

**Noise level:** 0

**Parallel imaging:** syngo GRAPPA, acceleration factor = 2

**Direction of diffusion gradients:** 3-scan trace

Typical FOV with rectangular FOV

Typical resolution, pixel size

### Contact

Farhood Saremi, M.D.  
Professor of Radiology and Medicine  
Chief, Cardiothoracic Division  
Dept. of Radiological Sciences  
University of California (UCI)  
Medical Center  
101 City Drive  
Irvine, CA 92868  
USA  
fsaremi@uci.edu